Check for updates

# Green synthesis of starch-capped $Cu_2O$ nanocubes and their application in the direct electrochemical detection of glucose†

Antonio Jiménez-Rodríguez, [a] Eduardo Sotelo, [a] Lidia Martínez, [b] Yves Huttel, [b] María Ujué González, [c] Alvaro Mayoral, [def] José Miguel García-Martín, [c] Marcelo Videa [*a] and Jorge L. Cholula-Díaz [*a]

Glucose determination is an essential procedure in different fields, used in clinical analysis for the prevention and monitoring of diabetes. In this work, modified carbon paste electrodes with $Cu_2O$ nanocubes ($Cu_2O$ NCs) were developed to test electrochemical glucose detection. The synthesis of the $Cu_2O$ NCs was achieved by a green method using starch as the capping agent, obtaining cubic-like morphologies and particle sizes from 227 to 123 nm with increasing amounts of the capping agent, as corroborated by electron microscopy analysis. Their crystalline structure and purity were determined by X-ray diffraction. The capability of starch as a capping agent was verified by Fourier-transform infrared spectroscopy, in which the presence of functional groups of this biopolymer in the $Cu_2O$ NCs were identified. The electrochemical response to glucose oxidation was determined by cyclic voltammetry, obtaining a linear response of the electrical current as a function of glucose concentration in the range $100-700$ μM, with sensitivities from 85.6 to 238.8 μA $mM^{-1}$ $cm^{-2}$, depending on the amount of starch used in the synthesis of the $Cu_2O$ NCs.

## 1 Introduction

Glucose quantification is required due to its importance in health and food industries, where this monosaccharide serves as an indicator in quality control,[1] and for clinical analysis and diagnosis.[2] Its quantification in industrial applications is usually carried out by near infrared (NIR) spectroscopy, which is not an adequate technique for clinical routine analysis.[3] Hence, ample research has been conducted to find more sensitive and reliable alternative techniques for routine glucose quantification, which can further improve diabetes diagnosis, a disease that could affect 5.9 billion people by 2035.[4]

Glucose monitoring methods are classified according to the type of technology applied to detect the biomarker. In a broad sense, there are optical, thermal, acoustic and electrochemical methods. Although each technology is nowadays commercially available, the electrochemical-based methods are the gold standards for calibration of other glucose meters and at central laboratories.[5] Currently, electrochemical techniques for glucose detection implement the glucose oxidase enzyme (GOx), which can selectively oxidize glucose in the presence of molecular oxygen ($O_2$),[6] producing gluconolactone and hydrogen peroxide ($H_2O_2$).[7] The latter is quantified amperometrically, achieving an indirect glucose quantification.[3] Nevertheless, the intrinsic nature of enzymes – in particular their structural changes due to physical treatments – the thermal history during the sensor assembly or chemical modifications due to pH variations,[8] may alter the reproducibility of the detection method. Furthermore, conventional devices for glucose monitoring are based on invasive methods, which require a certain amount of blood to be drawn out of the body by finger-pricking, making this method painful and uncomfortable for diabetes patients.[5,9] Hence, there is great interest in non-enzymatic glucose sensors that are based on the direct glucose oxidation over a working electrode without the participation of an enzyme;[10] these novel biosensors should minimize the risks and inconvenience of the invasive methods. For these reasons, noninvasive, accurate,

[a] *School of Engineering and Sciences, Tecnologico de Monterrey, Eugenio Garza Sada 2501, Monterrey 64849, NL, Mexico. E-mail: mvidea@tec.mx; jorgeluis.cholula@tec.mx*

[b] *Materials Science Factory, Instituto de Ciencia de Materiales de Madrid, ICMM-CSIC, Sor Juana Inés de la Cruz 3, Madrid 28049, Spain*

[c] *Instituto de Micro y Nanotecnología, IMN-CNM, CSIC (CEI UAM+CSIC), Isaac Newton 8, Tres Cantos 28760, Spain*

[d] *Instituto de Nanociencia y Materiales de Aragón (INMA), CSIC-Universidad de Zaragoza, Pedro Cerbuna, 50009, Zaragoza, Spain*

[e] *Center for High-Resolution Electron Microscopy (ChEM), School of Physical Science and Technology (SPST), ShanghaiTech University, 393 Middle Huaxia Road, Pudong, Shanghai, 201210, China*

[f] *Laboratorio de Microscopias Avanzadas (LMA), Universidad de Zaragoza, Spain*

† Electronic supplementary information (ESI) available: XRD patterns of six independent replicates of sample $Cu_2O$-NCs-1. EDX analysis of the four $Cu_2O$ NCs samples. XPS analysis of samples $Cu_2O$-NCs-0 and $Cu_2O$-NCs-5. Non-linear fits of the electrochemical glucose determination by CV. See DOI: 10.1039/d0ra10054d

portable and low-cost glucose monitoring devices to control diabetes are highly demanded. In this regard, saliva is very attractive as a biomedium for non-enzymatic electrochemical glucose sensors.[11]

Nanomaterials of noble metals like Au and Pt, as well as their alloys (PtAu and PtRu), have been investigated for glucose determination due to their catalytic activities in electrochemical processes.[4] However, the application of these metals as electrodes in sensors is restrained by their high cost,[7] and possible surface poisoning by intermediates such as carbon monoxide (CO) and chloride ions ($Cl^-$) that may be present in the sample.[12] These setbacks have prompted the search for substitutes that maintain the same performance and reduce costs.

Nanostructured transition metal oxides are promising materials for the non-enzymatic detection of glucose, due to their chemical stability, catalytic activity, particle size control, and biological compatibility.[10] Cuprous oxide ($Cu_2O$) has been investigated for its application as a glucose sensor using direct electrochemical methods because of its catalytic activity, chemical and electrochemical stability, and lower cost than noble metals.[6,13–15] Particularly, $Cu_2O$ nanocubes ($Cu_2O$ NCs) are very attractive due to their higher electrocatalytic activity in electrochemical processes like the oxygen reduction reaction (ORR).[16] For these reasons, the implementation of this type of nanostructure as a non-enzymatic glucose sensor may be very advantageous.

In general, $Cu_2O$ NCs synthesis has been reported mainly by wet routes that include the control of these main factors: copper precursor, reducing agent and capping agent. The capping agent, such as polyethylene glycol (PEG) and polyvinylpyrrolidone (PVP), modifies the particle size and the morphology of the nanomaterial.[16–19] Furthermore, common reducing agents in the synthesis of nanomaterials are hydrazine, sodium borohydride ($NaBH_4$), and dimethylformamide (DMF), which pose environmental and biological risks.[20,21] According to Duan *et al.*,[22] a green chemistry approach for a synthesis method should incorporate at least three factors: the use of nontoxic capping agents, less hazardous reducing agents, and the selection of environmentally benign solvents.

Starch is considered one of the most convenient stabilizer agents among the abundant, biocompatible, and renewable biopolymer materials for the synthesis of nanoparticles.[23] This biopolymer has been used for the synthesis of diverse nanoparticles such as metal and metal oxides due to its hydroxyl groups (–OH) that interact with the surface atoms of the nanomaterials.[24–29] Despite the synthesis of $Cu_2O$ nanostructures using starch as both the reducing and dispersing agent having been previously reported,[30–32] to the best of our knowledge, the application of starch–$Cu_2O$ nanocomposites as electrocatalysts for the direct sensing of glucose are yet to be evaluated.

The present work reports a highly reproducible green synthesis of $Cu_2O$ NCs using Benedict's reagent as the copper precursor, D-(+)-galactose as the reducing agent and starch as the capping agent. The aim of this project was to study the effect of starch as the capping agent on the physical and chemical properties of the $Cu_2O$ NCs, *i.e.*, crystalline structure, chemical composition, particle size, and the electrochemical activity of the nanomaterial in the oxidation of glucose. To achieve these goals, the amount of starch used in the synthesis of the $Cu_2O$ NCs was varied and the resulting nanomaterials were thoroughly characterized. Finally, the glucose sensing properties of the starch–$Cu_2O$ nanocomposites were tested by cyclic voltammetry.

## 2 Materials and methods

### 2.1 Materials

The reactants used in the green synthesis of $Cu_2O$ nanocubes were copper(II) sulfate pentahydrate ($CuSO_4 \cdot 5H_2O$; ≥98%, Sigma-Aldrich), sodium citrate dihydrate ($Na_3Cit \cdot 2H_2O$; ≥99%, Sigma-Aldrich), D-(+)-galactose (≥99%, Sigma-Aldrich), sodium carbonate ($Na_2CO_3$; ≥99.5%, Sigma-Aldrich), sodium hydroxide (NaOH; 98.4%, CTR Scientific, Monterrey, N.L., Mexico) and starch (Reagent Grade, CTR Scientific, Monterrey, N.L., Mexico). For the electrochemical experiments, the following chemicals were utilized: graphite (<20 micron, reagent grade, Sigma-Aldrich), paraffin wax (Reagent grade, Sigma-Aldrich), D-glucose (≥99.5%, Sigma-Aldrich), and acetone (Reagent Grade, CTR Scientific, Monterrey, N.L., Mexico). Deionized water ($\rho$ = 18 MΩ cm) was used in the synthesis of $Cu_2O$ nanocubes, as well as for all the following procedures described below. All the glassware and stirring bars used were kept under an 11.11% v/v HCl solution for 24 hours, followed by immersion in a KOH/EtOH solution for the same amount of time and then rinsed with water prior to use.

### 2.2 Synthesis of $Cu_2O$ nanocubes

The methodology for the synthesis of $Cu_2O$ NCs is a modification to the method reported by Markina *et al.*[33] First, stock solutions were prepared. The preparation of the modified Benedict's reagent consists of mixing a solution of 300.0 mg of $CuSO_4 \cdot 5H_2O$ in 1 mL of water and a solution of 346.2 mg of $Na_3Cit \cdot 2H_2O$ and 200.2 mg of $Na_2CO_3$ in 4 mL of water. A fresh 1% w/v aqueous starch solution was prepared and heated to 70 °C. Finally, a 40% w/v D-(+)-galactose aqueous solution was prepared.

The reaction consisted of adding 1 mL of 0.1 M NaOH to a glass vial and enough water to reach a volume of 10 mL. Then 0.2, 1 or 5 mL of the starch solution, 50 μL of 40% w/v galactose solution, and 200 μL of Benedict's reagent were added with a time lag of 5 min between them. The overall reaction was heated up to 95 °C, stirred at 500 rpm, and left for 15 min after the addition of Benedict's reagent. The resultant colloid was centrifuged three times for 10 min at 15 000 rcf. After each centrifugation process, the supernatant was discarded and the remaining pellet was redispersed in 10 mL of water with sonication.

### 2.3 Characterization of $Cu_2O$ nanocubes

**2.3.1 X-ray diffraction.** XRD was used both to verify the crystalline phase and in the determination of the crystallite size of the obtained copper oxide nanomaterials. Briefly,

a dispersion of 1 mL of the Cu$_2$O nanocubes was added dropwise onto a cover glass previously sonicated in methanol for 5 minutes and rinsed with sufficient water. The water was evaporated by heating on a hot plate at 90 °C. Diffractograms were obtained using a Rigaku Miniflex 600 diffractometer with a Cu-K$\alpha$ source ($\lambda = 1.5406$ Å) at 40 kV and 15 mA. The XRD patterns were acquired at room temperature with a step of 0.02° (2$\theta$) and a scan rate of 1° min$^{-1}$.

**2.3.2 Fourier-transform infrared spectroscopy.** Fourier-transform infrared (FTIR) spectroscopy was employed to verify the presence of starch on the Cu$_2$O NCs and thus confirm its use as capping agent. The sample preparation for this technique was the same as for XRD analysis. Spectra were obtained using a Perkin Elmer Spectrum 400 FTIR/FTNIR spectrometer in attenuated total reflectance (ATR) mode.

**2.3.3 Scanning electron microscopy.** Scanning electron microscopy (SEM) was used not only to determine the size and morphology of the Cu$_2$O nanostructures, but also to perform electron dispersive X-ray spectroscopy (EDX). The equipment used was an FEI Verios 460 field emission microscope. The sample preparation consisted of depositing the sample used for XRD analysis on a pin stub with a carbon tape; furthermore, an additional carbon tape was placed nearby the powder sample and the pin stub to assure conductivity. For the morphological study, the micrographs were obtained with 2 kV acceleration voltage and 25 pA electron beam current. For EDX characterization, an EDX detector (EDAX Octane Plus) coupled to the microscope is used. In this case, the parameters were 400 pA current and 15 kV acceleration voltage, in order to obtain information from all the relevant elements.

**2.3.4 Scanning transmission electron microscopy.** The Cu$_2$O NCs samples were analyzed by means of spherical aberration corrected scanning transmission electron microscopy (C$_s$-corrected STEM) using an annular dark field detector (HAADF). STEM inspection was performed using an FEI Titan XFEG transmission electron microscope equipped with a CEOS spherical aberration corrector for the electron probe. Prior to the experiments, the aberrations were corrected using a gold standard sample assuring a spatial resolution of 0.8 Å. For chemical analyses, the microscope was also fitted with a Gatan Tridiem energy filter (GIF) and with a silicon drift detector (SDD) Oxford energy dispersive X-ray spectrometer. The chemical information was acquired by means of EDX spectroscopy. For electron microscopy STEM inspection, the colloidal Cu$_2$O NCS were firstly sonicated to minimize particle agglomeration and a few drops of the colloid were deposited onto holey carbon nickel microgrids.

**2.3.5 X-ray photoemission spectroscopy measurements.** Samples grown with and without starch and deposited on thin glass substrates were introduced into an ultra high vacuum system for X-ray photoemission spectroscopy (XPS) characterization. The samples were first loaded in a vacuum load-lock chamber and then transferred in the XPS chamber with a base pressure in the low $10^{-10}$ mbar range. The chamber is equipped with a hemispherical electron energy analyzer (SPECS Phoibos 100 spectrometer) and an Al-K$\alpha$ (1486.29 eV) X-ray source. The angle between the hemispherical analyzer and the plane of the sample was 60°. Wide scan spectra were recorded using an energy step of 0.5 eV and a pass-energy of 40 eV, while specific core levels and Auger spectra (Cu 2p, Cu L$_3$M$_{45}$M$_{45}$, O 1s and C 1s) were recorded using an energy step of 0.1 eV and a pass-energy of 20 eV. The spectra were analyzed using CasaXPS software (Casa software Ltd, Cheshire, UK). The absolute binding energies (BE) of the photoelectron spectra were determined by referencing the Cu 2p core level peak at 932.7 eV. The contributions of the Al-K$\alpha$ satellite lines were subtracted.

**2.3.6 Electrochemical measurements.** Cyclic voltammetry was employed to observe the glucose redox processes associated with the Cu$_2$O NCs in basic media (0.1 M NaOH). First, a carbon paste electrode (CPE) was constructed with 25% w/w paraffin wax, 45% w/w graphite and 30% w/w Cu$_2$O NCs. The materials were dispersed in acetone in an ultrasound bath at a temperature above 60 °C. The paste was then transferred into a glass tube (5 mm I.D.) containing a Pt coil, which served as a current collector and was not in direct contact with the electrolyte. The CPE was polished on the surface of a paper until a uniform surface was obtained. Electrochemical experiments were performed on a Princeton Applied Research, EG&G 273A potentiostat/galvanostat. A conventional three-electrode configuration was used: saturated Ag|AgCl as the reference electrode, Pt wire as the counter electrode and the CPE as the working electrode. A solution of 0.1 M NaOH was used as the supporting electrolyte. The voltammograms were obtained at a scan rate of 20 mV s$^{-1}$ after 10 cycles, unless otherwise specified.

# 3 Results and discussion

## 3.1 Synthesis of the Cu$_2$O NCs

Cuprous oxide nanocubes (Cu$_2$O NCs) were obtained by a green synthesis method using Benedict's reagent as the copper source, galactose as the reducing agent and starch as the capping agent. During the final part of the reaction, the color of the dispersions changed from orange to a yellow-orange using a 1% w/v starch solution. A similar color was observed by Huang *et al.* in Cu$_2$O colloids obtained using sodium dodecyl sulfate surfactant.[34] Fig. 1a shows the effect of the capping agent on the color of the colloids, and Fig. 1b depicts the stability of the dispersions after 72 h aging at room temperature. A clear visual difference in the stability of the suspensions was observed, wherein the non-capped Cu$_2$O NCs (Cu$_2$O-NCs-0) completely precipitated in less than 30 min, the starch-capped Cu$_2$O NCs (Cu$_2$O-NCs-1) suspension was kept relatively stable after 72 h. These results are comparable with the effect of (3-aminopropyl) trimethoxysilane (APTMS) in the stability of copper nanopowders, conferring stability to the colloid within 72 h in comparison with the sedimentation of the bare nanomaterial.[35] In the case of the dispersions with 0.2, 1, and 5 mL of the starch solution (Cu$_2$O-NCs-0.2, Cu$_2$O-NCs-1 and Cu$_2$O-NCs-5, respectively), Fig. 1c, the relative stability increased as the amount of capping agent was increased (Fig. 1d). The same trend was observed in chitosan-capped silver nanoparticles, where the
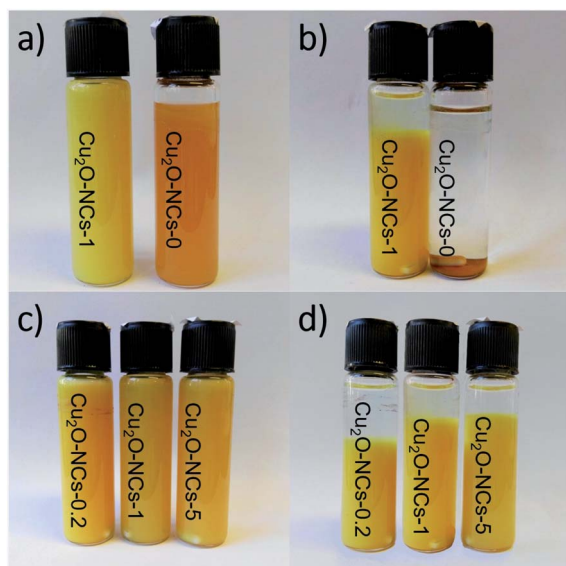
**Fig. 1** Cu$_2$O NCs synthesized using different amounts of a 1% w/v starch solution. (a) Colloid of Cu$_2$O NCs after using 1 mL of the starch solution (Cu$_2$O-NCs-1) and without the capping agent (Cu$_2$O-NCs-0); (b) stability of previous dispersions after 72 h at room temperature; (c) colloids obtained with 0.2 mL (Cu$_2$O-NCs-0.2), 1 mL (Cu$_2$O-NCs-1), and 5 mL (Cu$_2$O-NCs-5) starch solution; (d) stability of the previous colloids after 72 h at room temperature.

stability was increased by the amount of chitosan used as the capping agent.[36]

### 3.2 Structural characterization using XRD

The X-ray diffraction (XRD) patterns of the synthesized Cu$_2$O NCs are presented in Fig. 2 along with the Cu$_2$O reference diffractogram obtained from Mercury 4.0 Software[37] using experimental data from Kirfel and Eichhorn.[38] Diffraction peaks observed at $2\theta \approx 29.59, 36.45, 42.34, 61.42, 73.58$ and $77.43°$ were indexed to (110), (111), (200), (220), (311) and (222) crystallographic planes that correspond to the expected diffraction peaks for cubic Cu$_2$O (space group $Pn\bar{3}m$).[38]

Comparing the experimental XRD patterns of Cu$_2$O synthesized with and without starch, the formation of Cu$_2$O without any impurities from the reagents used in the synthesis, can be verified. The main difference in these patterns is the broadening of the peaks, which is related to the size of the crystallite of the sample, as described in Scherrer's equation:[39,40]

$$d = K\lambda/\beta \cos \theta \qquad (1)$$

where $d$ is the crystallite size, $K$ is the Scherrer's constant (usually $K = 0.9$), $\lambda$ is the wavelength of the X-ray, $\beta$ is the full width at half maximum (FWHM) of the diffraction peak and $\theta$ is the diffraction angle.

As described in eqn (1), the size of the crystallite is inversely proportional to FWHM of the diffraction peak; thus, a large value of FWHM corresponds to a smaller crystallite size. Table 1 provides a summary of the values for the crystallite size and lattice parameter ($a$). Due to the effect of starch in reducing the
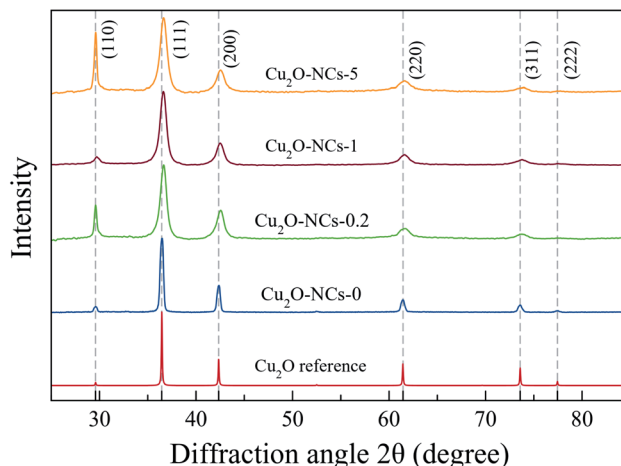


**Fig. 2** XRD patterns of Cu$_2$O nanocubes synthesized without starch (Cu$_2$O-NCs-0) and with different amounts of 1% w/v starch solution (0.2, 1 and 5 mL for Cu$_2$O-NCs-0.2, Cu$_2$O-NCs-1 and Cu$_2$O-NCs-5, respectively). Miller indexes corresponding to cubic Cu$_2$O with space group $Pn\bar{3}m$.[38]

size of the Cu$_2$O NCs, the broadening of the diffraction peaks was used as a parameter to study the concentration effect of this biopolymer on the size of the nanomaterials. To analyze this effect, a comparison was drawn from two variations of the 1% w/v starch solution volume (0.2 and 5 mL) and the standard synthesis (1 mL), as shown in Fig. 2. The ratio of the intensity of the (220) peak to that of the (200) peak was in the range of 0.30–0.35, in agreement to the values found in Cu$_2$O NCs.[34] However, a significant difference found among these XRD patterns appears in the relative intensity between the (110) and (111) peaks in the samples Cu$_2$O-NCS-0.2 and Cu$_2$O-NCs-5, which may indicate an *anomalously* crystallographic growth orientation exposing the {110} facets. As mentioned by Tang et al.,[41] the intensity of diffraction peaks in XRD patterns may exhibit the intrinsic abundance of crystal planes of the Cu$_2$O structure. Our experimental results need further investigation to clarify this variance in the observed relative intensity of the referred diffraction peaks.

To confirm the reproducibility of the proposed synthesis methodology, six replicates ($N = 6$) of the synthesis of the Cu$_2$O NCs using 1 mL of the starch solution were prepared and analyzed by XRD. In the ESI, Fig. S1† shows the XRD patterns of the replicates, which are similar to each other, proving the reproducibility of the synthetic method.

**Table 1** Calculated lattice parameter ($a$) and crystallite size of Cu$_2$O NCs with and without starch

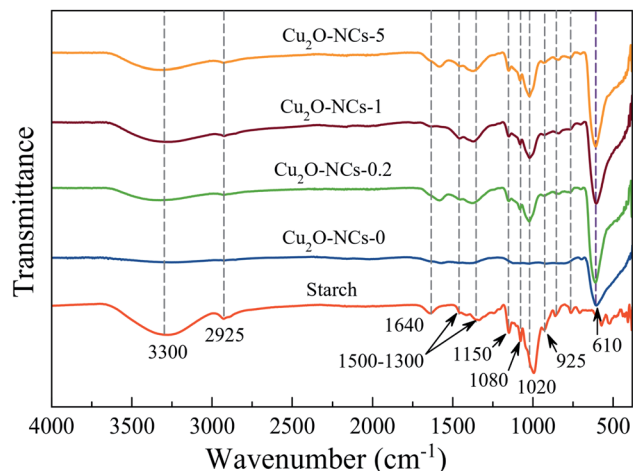| Sample | Lattice parameter ($a$) (Å) | Crystallite size (nm) |
|---|---|---|
| Cu$_2$O-NCs-0 | $4.26 \pm 0.01$ | $22.3 \pm 3.5$ |
| Cu$_2$O-NCs-0.2 | $4.25 \pm 0.01$ | $9.2 \pm 1.6$ |
| Cu$_2$O-NCs-1 | $4.25 \pm 0.01$ | $8.8 \pm 1.6$ |
| Cu$_2$O-NCs-5 | $4.25 \pm 0.01$ | $8.1 \pm 1.6$ |

**Fig. 3** FT-IR spectra of $Cu_2O$ nanocubes synthesized using different amounts of starch. Starch powder was measured as the reference.

### 3.3 Capping ability of starch characterized by FT-IR spectroscopy

Comparing the FT-IR spectra of the $Cu_2O$ NCs synthesized with and without starch, to the spectrum of this biopolymer, which was taken as the reference, confirms the adsorption of starch on the surface of the $Cu_2O$ nanostructures, as shown in Fig. 3. The spectra of the three different starch-capped $Cu_2O$ NCs samples showed the characteristic bands of starch: a broad band around $3300$ $cm^{-1}$ attributed to the O–H stretching mode (remarking that starch presents a more intense band than those in nanocubes, which may be related to the decrease of free hydroxyl groups due to their linkage to the nanocubes).[23] A band around $2925$ $cm^{-1}$ corresponding to the C–H stretching;[42] $1640$ $cm^{-1}$ related to tightly bound water in starch;[43] vibrational bands in the region of $1500$–$1300$ $cm^{-1}$ attributed to C–H bending and deformation;[44] $1150$ $cm^{-1}$ is related to vibrations of the glucosidic C–O–C bond.[45] The bands at $1080$ and $1020$ $cm^{-1}$ are characteristic of the anhydroglucose ring O–C stretch.[43] The band at $925$ $cm^{-1}$ is assigned to vibrational modes of $\alpha$ $1 \rightarrow 4$ skeletal glycoside bonds[45] and bands below $800$ $cm^{-1}$ were related to skeletal mode vibrations of the glucose pyranose ring.[44] Thus, the capping capability of starch for $Cu_2O$ NCs was proven. Besides the characteristic functional groups of starch, a band at $610$ $cm^{-1}$ relates to the Cu–O bond in $Cu_2O$ in all four samples.[46]

### 3.4 Particle size and morphology characterization of $Cu_2O$ nanocubes by SEM and TEM

SEM imaging allowed the observation of the cubic morphology of the nanomaterials as well as their particle sizes by measuring the length of the cube edge. For comparison purposes, only cubic morphologies found in the samples were counted to construct the particle size distributions ($n = 100$).

The SEM images and the respective particle size distribution of the four $Cu_2O$ NCs samples are shown in Fig. 4 and S2 (ESI†). In Fig. 4a and b, the SEM images of the Cu-based nanomaterial synthesized in the absence of starch ($Cu_2O$-NCs-0) shows relatively smooth facets with different particle shapes, such as well-defined cuboctahedra, truncated cubes, quasi-spherical particles, and cubes with an average particle size of $227 \pm 69$ nm. The SEM images in Fig. 4c and d show the effect of adding 0.2 mL of 1% w/v starch solution to the reaction ($Cu_2O$-NCs-0.2), observing a cubic-like morphology with rough surfaces. Actually, it was observed that each nanocube is composed of self-assembled $Cu_2O$ aggregates forming a highly polycrystalline structure. The average particle size for this sample was $179 \pm 21$ nm. Fig. 4e and f exhibit the resulting $Cu_2O$ nanocubes produced with a higher volume of the starch solution (1 mL, $Cu_2O$-NCs-1), which also presents rough surfaces and smaller nanocubes of $143 \pm 20$ nm. Finally, Fig. 4g and h correspond to the $Cu_2O$ NCs resulting from the addition of 5 mL of the starch solution ($Cu_2O$-NCs-5) with even smaller average particle sizes of $123 \pm 20$ nm. These results confirmed that the amount of starch in the synthesis determines the average size of $Cu_2O$ NCs,
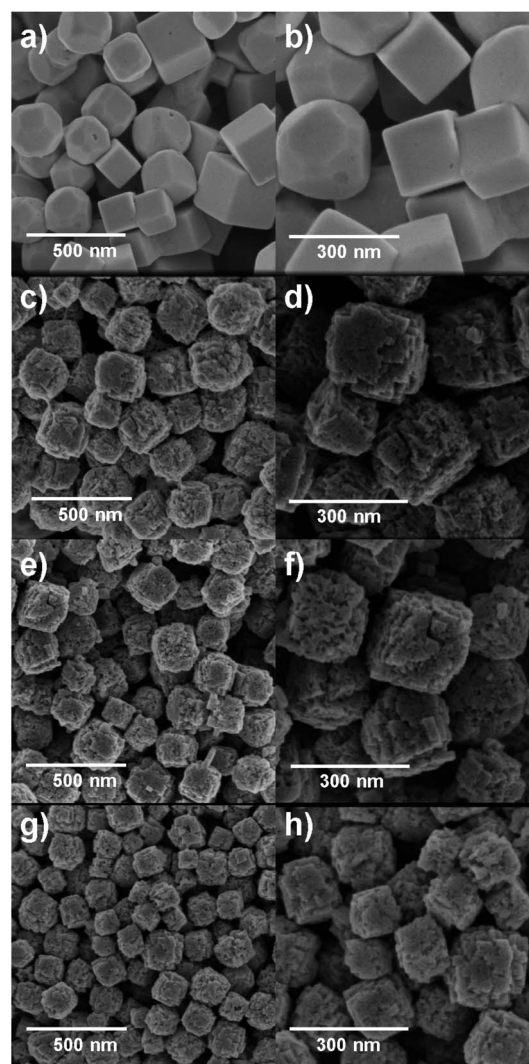


**Fig. 4** SEM images of $Cu_2O$ NCs varying the amount of 1% w/v starch solution in their synthesis. (a and b) without starch; (c and d) 0.2 mL; (e and f) 1 mL; (g and h) 5 mL.
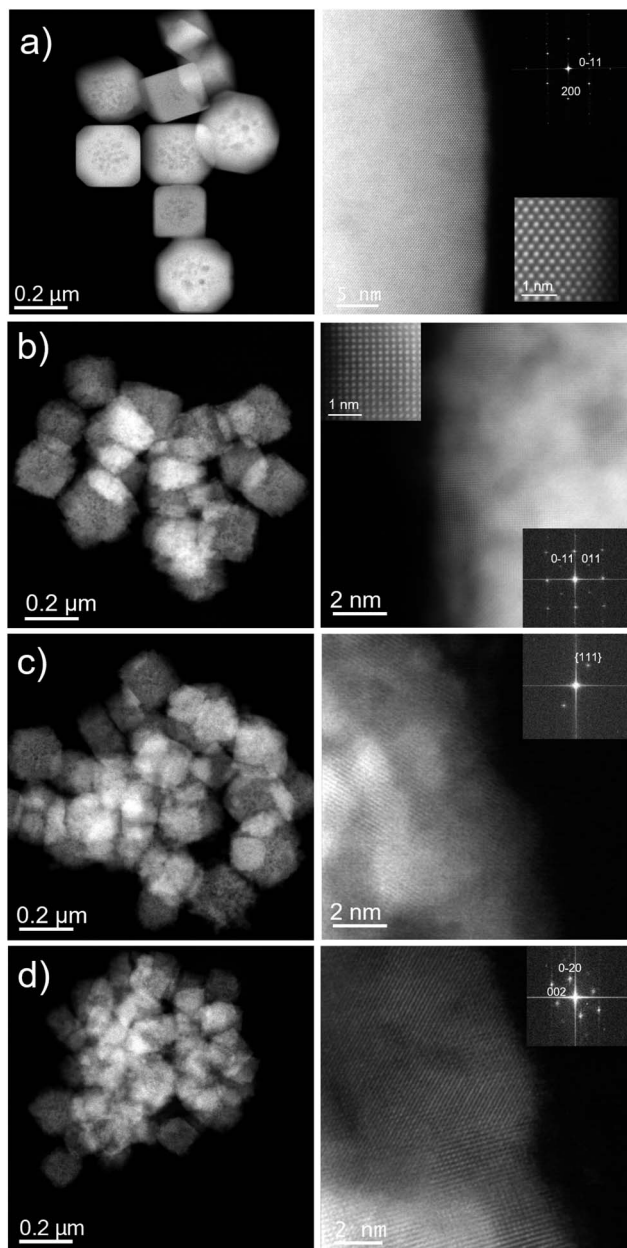
**Fig. 5** $C_s$-corrected STEM-HAADF of samples (a) $Cu_2O$-NCs-0, (b) $Cu_2O$-NCs-0.2, (c) $Cu_2O$-NCs-1 and (d) $Cu_2O$-NCs-5. The left column corresponds to the low magnification images, while the right one displays the atomic resolution information. The FDs are shown in the insets.

*i.e.*, higher amounts of the starch solution prompt smaller NCs. These experimental observations were in disagreement with a similar nanosystem reported by Sun *et al.*, in which the mean particle size of $Cu_2O$ octahedral microcrystals increased from 1.60 to 3.85 μm upon addition of starch as the reducing and dispersing agent.[32] On the other hand, reduction of the particle size as a function of starch was presented on starch-capped Ag nanoparticles.[47] This effect may be attributed to the strong interaction of hydroxyl groups (–OH) of starch that cause effectual passivation of the surfaces and consequent

suppression of the growth of the $Cu_2O$ NCs. Moreover, it has been reported that structure-directing agents with high molecular weights ($M_w$), such as polyethylene glycol with $M_w =$ 20 000 g mol$^{-1}$ (PEG-20000), yielded hierarchically structured $Cu_2O$ NCs with rough surfaces and undefined edges comprising self-assembled 5 nm $Cu_2O$ nanocrystallites.[48] In contrast, the use of a lower molecular weight, PEG-400 ($M_w = 400$ g mol$^{-1}$), resulted in the formation of smooth and regular $Cu_2O$ NCs.[48] In a similar manner, the use of starch, a biopolymer with a high molecular weight ($M_w \sim 10^6$ g mol$^{-1}$), could promote the growth of irregular $Cu_2O$ NCs that may resemble hierarchical-like nanostructures. In fact, Chen *et al.* reported the synthesis of nanoparticle-aggregated octahedron-like $Cu_2O$ nanostructures with the assistance of starch acting as the reducing agent.[30]

Low-magnification $C_s$-corrected STEM-HAADF of the nanomaterial synthesized with no starch ($Cu_2O$-NCs-0) is presented in Fig. 5a, left column, where very well faceted particles with sizes in the range 200–300 nm with cubic and cuboctahedral morphologies can be observed. A closer observation of the edge is depicted in Fig. 5a, right column, proving the excellent crystallinity of the $Cu_2O$ nanostructures. Here, the atomic distribution is evidenced along the [110] orientation, see the Fourier
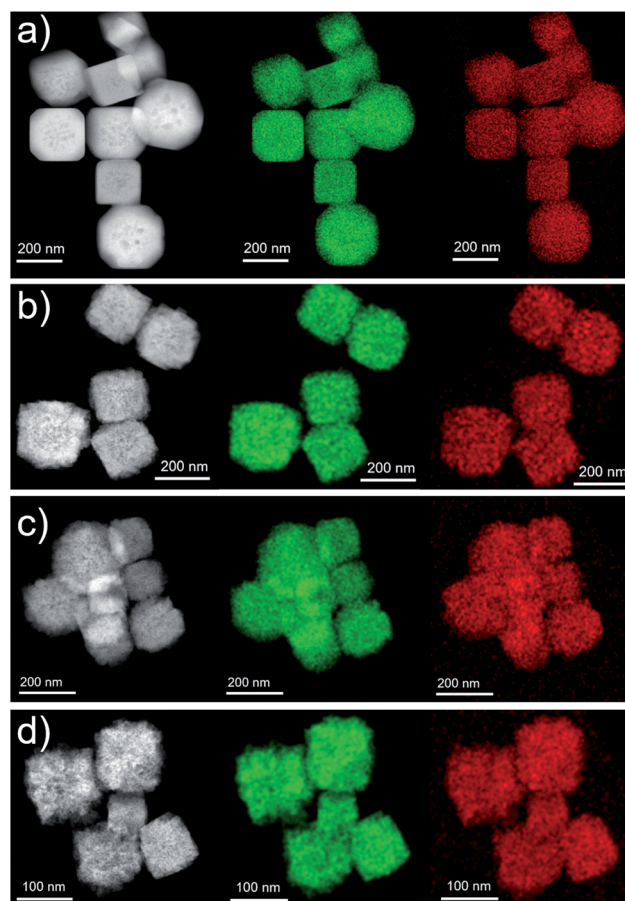


**Fig. 6** Chemical analysis of (a) $Cu_2O$-NCs-0, (b) $Cu_2O$-NCs-0.2, (c) $Cu_2O$-NCs-1 and (d) $Cu_2O$-NCs-5. Each analysis is composed by a STEM-HAADF image that contains several nanocubes and the corresponding Cu (green) and O (red) maps.

     

**Paper**

diffractogram (FD) in the inset, top right of Fig. 5a. The FD could be indexed assuming $Pn\bar{3}m$ symmetry with a calculated cubic unit cell of $a = 4.25$ Å, in agreement with the values found by XRD analysis (Table 1) and reported in the literature for $Cu_2O$ cubes.[41] A magnified image of the atomic configuration is shown in the inset on the bottom right of Fig. 5a, right column.

The same analysis was carried out for the $Cu_2O$ nanocubes synthesized with starch. Fig. 5b–d (left column) reveals, as already evidenced by SEM analysis, the reduction of the particle size as a function of starch solution used in the synthesis and the formation of less defined nanocubes. Each nanocube is composed of small single crystals (crystallites) giving an overall polycrystalline material. The structure of the three samples was in agreement with the cubic $Pn\bar{3}m$ $Cu_2O$ symmetry[38] and the corresponding FDs have been inserted within the high-magnification images (Fig. 5b–d, right columns). A clear atomic observation along the [100] projection is depicted in Fig. 5b (high-resolution inset top left), as a representative example of the crystalline nature of these domains.

### 3.5 Characterization of the chemical composition of the $Cu_2O$ NCs by EDX and XPS

In order to gain information on the chemical composition of the samples, EDX analyses (coupled with SEM imaging) were done (Fig. S3–S6†). As no standard sample of a similar system with known composition to refer to in EDX measurements was available, the obtained atomic contents were semi-quantitative. However, they could provide comparisons and evolution between the different samples. In all the samples Cu, O, and C stand for at least 94% of the composition, and the remaining <4% of the composition found in the EDX spectra is due to Si (from the substrate), as well as minor and trace constituents coming from the reactants in the synthesis. Fig. S7† shows the ratio between the contents of Cu and C as well as the ratio between Cu and O as a function of the amount of starch solution used in the reaction. It can be observed that the ratios decrease as the concentration of starch increases, as expected: Cu and part of the O can be ascribed to the $Cu_2O$

**Table 2** Composition of the $Cu_2O$ NCs samples extracted from the wide energy range scans

| | Composition atomic% | | | | |
| --- | --- | --- | --- | --- | --- |
| | Cu | C | O | N | Na |
| $Cu_2O$-NCs-0 | 21.1 | 44.3 | 31.7 | — | 2.9 |
| $Cu_2O$-NCs-5 | 17.7 | 42.1 | 39.8 | 0.4 | — |

nanostructures, whereas C and the rest of the O can be ascribed to starch.

A more extensive chemical elemental analysis was completed by means of EDX mapping on individual $Cu_2O$ nanostructures. In all cases, chemical maps were obtained for Cu and O, as no other element was identified. For each case, a chemical map is presented proving the homogeneous composition is present in every sample (Fig. 6), and single-nanocube chemical maps (Fig. S8†) display that the composition of the nanostructure was homogeneous along the individual nanostructure. In addition, the spectra, where the chemical maps were extracted from, are depicted in Fig. S8.†

The XPS characterization was performed on the two extremes on the $Cu_2O$ NCs set of samples: grown without starch and with 5 mL of the 1% w/v starch solution. Fig. 7 shows the wide energy range scan spectra of both samples, and Table 2 gives the composition of the samples extracted from their analyses. In the two samples Cu, O and C were detectable. In addition, Na was detected in the sample prepared without starch, and traces of N were found in the sample without starch. The main difference in elemental composition between the samples relies on the amount of oxygen, as the sample with starch presents 8% more than the sample without starch. The presence of Na is understandable due to the reactants used for the synthesis of the $Cu_2O$ NCs, and the higher content of O in the sample grown with starch is certainly due to starch capping as demonstrated by the FT-IR spectra (Fig. 3). As XPS is a surface sensitive technique, the starch capping induces a lowering of the Cu signal in the sample that is capped with starch (17.7%) as compared to the sample prepared without starch (21.1%), once again in agreement with FT-IR results.

Detailed analysis of the Cu 2p core level peak (Fig. S9a†) evidenced a shoulder in the main peak at 934.5 eV, and smaller contributions at 941.3 eV and 943.9 eV that are characteristic of CuO.[49,50] In addition, the $Cu_{LMM}$ Auger peak (Fig. S9b†) presents the characteristic shape of CuO.[50] Therefore, Cu in both samples is oxidized in the form of $Cu^{2+}$. Hence, XPS, which is a surface analysis technique, only detects CuO. Combining this result with that obtained in the XRD, high-resolution TEM and FD analyses, we can infer that the nanocubes are mainly formed of $Cu_2O$ and exhibit an outer thin shell of CuO. The formation of such a shell can be ascribed to natural oxidation in ambient conditions.

Fig. S10† presents the C 1s and O 1s core level peaks of the samples. Significant changes were found on both core level peaks. In the case of the C 1s, the peaks have been fitted using four components, which correspond to C–C/C–H bonds at 285
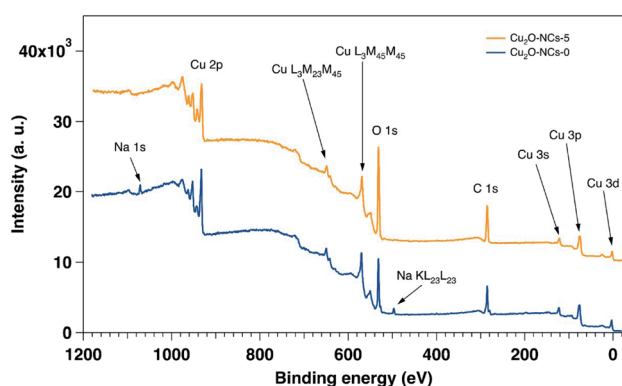


**Fig. 7** Wide energy range scans of the samples with and without starch ($Cu_2O$-NCs-5 and $Cu_2O$-NCs-0, respectively). The intensity offset of the spectrum corresponding to the sample grown with starch has been added for the sake of comparison.
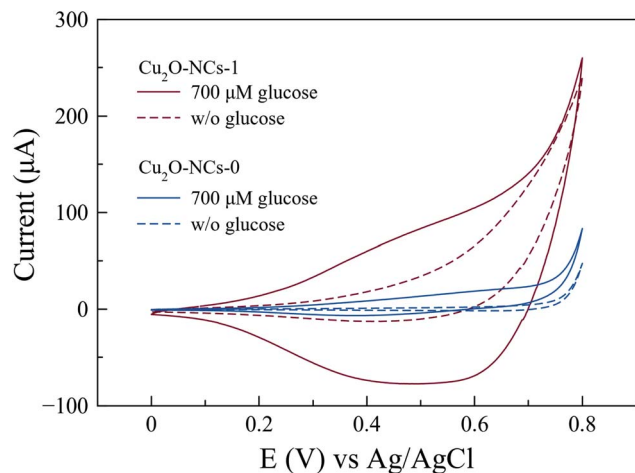
Fig. 8 Cyclic voltammograms for the oxidation of 700 µM glucose in 0.1 M NaOH with $Cu_2O$ NCs synthesized with 1 mL of 1% w/v starch solution ($Cu_2O$-NCs-1) and without starch ($Cu_2O$-NCs-0).
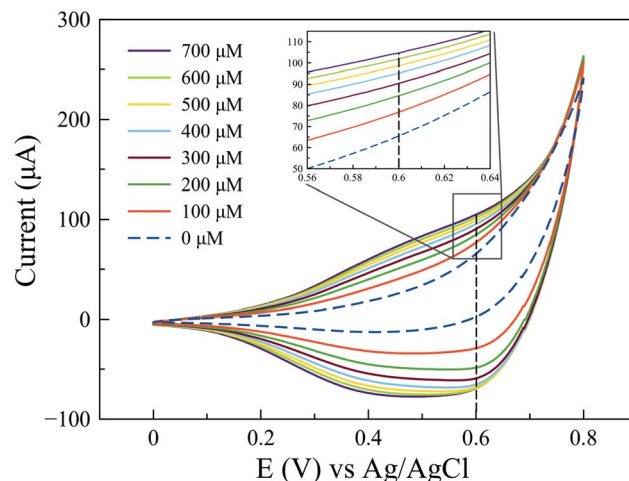


Fig. 9 Cyclic voltammograms obtained at different concentrations of glucose from 100 to 700 µM using the $Cu_2O$-NCs-1 sample.

± 0.2 eV; C–O/C–N bonds at 286.3 ± 0.2 eV; C=O bonds at 288.1 ± 0.2 eV; and O–C=O bonds at 289 ± 0.2 eV. These four components are typical of organic compounds.[51] As expected, the sample with starch presented a larger proportion of C–O bonds in comparison to the sample without starch, but also two times more C=O bonds.

In the case of the O 1s core level peak, two components were used in an attempt to make a fitting with the minimum possible number of components. The first component (O1) is centered at 530.9 ± 0.1 eV and the second (O2) at 532.6 ± 0.2 eV. Both components could be related to the presence of C–O–C and $CH_2OH$ residues. The oxygen component related to the presence of CuO should appear at lower binding energy than the O1 component (530.3 eV and the CuOH at 531.8 eV [50]). If the fitting is forced to include these components, keeping the same FWHM in all of them (Fig. S11†), in the case of the sample without starch, 73% of the oxygen could be related to the presence of CuOH, but without any indication of the oxide component. Basically, the sample with starch keeps the same fitting presented in Fig. S10,† as only 0.4% of the oxygen could be related to CuO, and no evidence of CuOH was found. In conclusion, the Cu of both samples is in the form of $Cu^{2+}$, and probably in the form of hydroxide in the sample with no starch.

### 3.6 Electrochemical glucose determination by cyclic voltammetry

Electrochemical experiments were performed using a carbon-paste composite working electrode containing graphite and the $Cu_2O$ NCs ($Cu_2O$ NCs/CPE) to evaluate the specific electrochemical activity of these nanomaterials in glucose oxidation. Fig. 8 shows the cyclic voltammetry responses of $Cu_2O$ NCs synthesized with and without starch in the presence (and absence) of 700 µM glucose in a 0.1 M NaOH electrolyte. For the $Cu_2O$ NCs synthesized without starch ($Cu_2O$-NCs-0), the oxidation of glucose was observed at an onset voltage of *ca.* 0.60 V *vs.*

Ag|AgCl as an increment in the current of 20.3 µA when compared to the blank experiment in the absence of glucose. When using the working electrode with the sample $Cu_2O$-NCs-1, a significant increase in current occurs at 0.60 V *vs.* Ag|AgCl showing a current almost 6 times larger than $Cu_2O$-NCs-0. This behavior was ascribed to the glucose oxidation process, which is similar to the results reported by Felix *et al.*,[13] where the current is related to the oxidation of glucose to gluconolactone occurring at the same moment as the conversion of Cu(II) to Cu(III) that catalyzes the previous reaction. Furthermore, the notorious difference in current at a given applied voltage may imply a higher activity due to the smaller nanocubes in $Cu_2O$-NCs-1 (mean particle size of 143 nm) in comparison with the $Cu_2O$ NCs synthesized without starch (mean particle size of 230 nm). Hence, more active sites to carry glucose oxidation are present in $Cu_2O$-NCs-1 with a consequent increment in the obtained current.[52]

Since a better response for glucose oxidation is expected at a larger surface area, the $Cu_2O$-NCs-1 sample was further analyzed. The cyclic voltammetry obtained at different concentrations of glucose are represented in Fig. 9, where the glucose concentration analyzed ranged from 100 to 700 µM, demonstrating the current dependence on glucose concentration. A correction of the baseline of the oxidation processes (positive currents) was done to obtain anodic currents related to glucose oxidation by the subtraction of the blank from the results of different glucose concentrations. This procedure conferred at the same time the removal of the signal from the $Cu_2O$ NCs to observe only glucose oxidation. Current at a potential of 0.60 V *vs.* Ag|AgCl was chosen, as previously mentioned, due to glucose oxidation processes. These currents were plotted as a function of the glucose concentration from 100 to 700 µM to obtain the calibration curve shown in Fig. 10c, each point on the calibration curve represents the average value for three independent measurements with error bars representing the standard deviation for each set of measurements. The correlation coefficient ($R^2$) for the calibration curve was
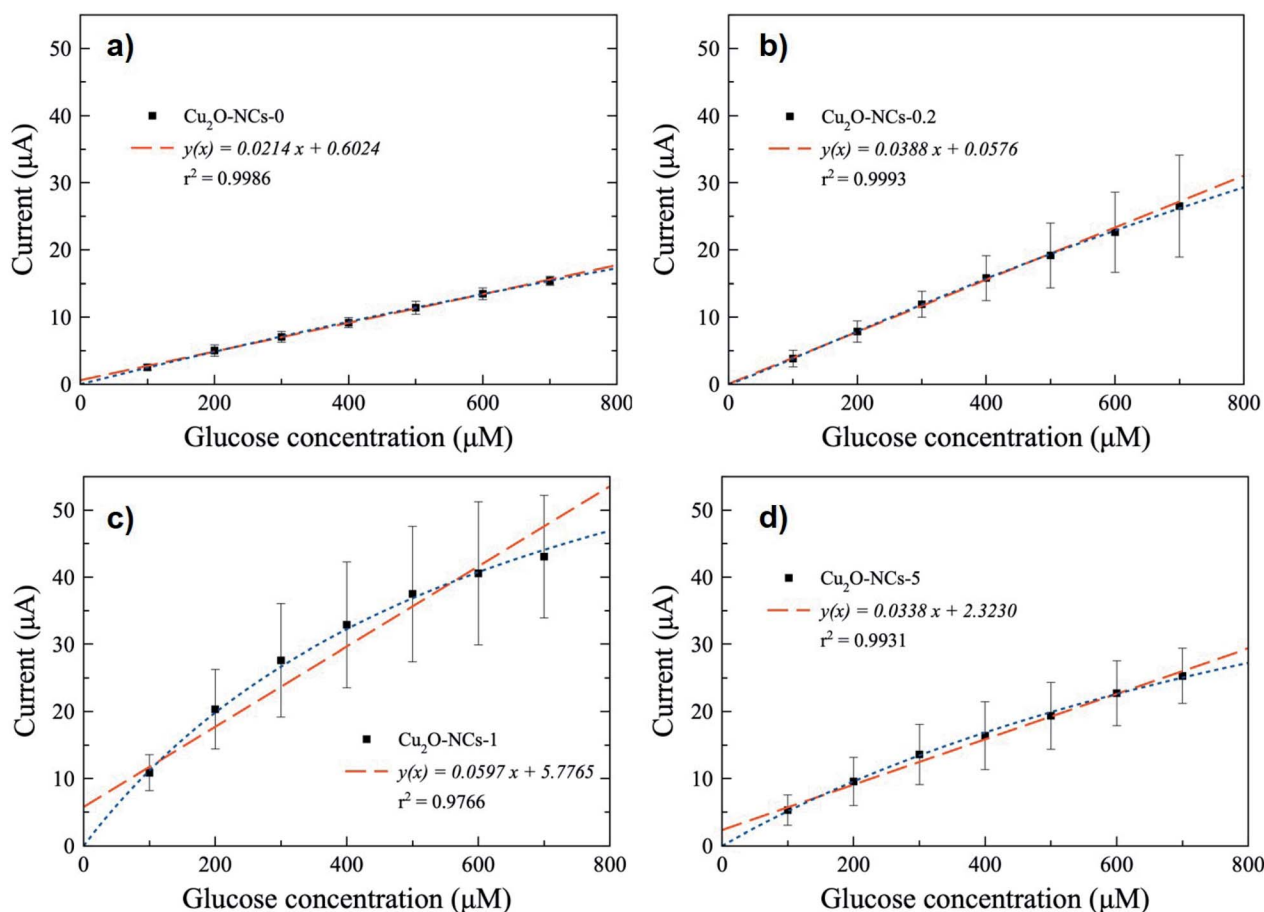
**Fig. 10** Calibration curves of glucose obtained at 0.60 V *vs.* Ag|AgCl with (a) $Cu_2O$ NCs without starch ($Cu_2O$-NCs-0) and with different amounts of a 1% w/v starch solution: (b) 0.2 mL ($Cu_2O$-NCs-0.2); (c) 1 mL ($Cu_2O$-NCs-1) and (d) 5 mL ($Cu_2O$-NCs-5). The dashed and dotted lines correspond to linear and non-linear fits, respectively, obtained from data in the range from 100 to 700 μM. Each point on the calibration curve represents the average value for three independent measurements with error bars showing the standard deviation for each set of measurements.

**Table 3** Comparison of analytical parameters of non-enzymatic glucose sensors based on $Cu_2O$ nanomaterials. NCs: nanocubes; GCE: glassy carbon electrode; RGO: reduced graphene oxide; GN: graphene nanosheets; NHs: nanohexagons; CPE: carbon paste electrode

| Electrode matrix | Linear range (mM) | Sensitivity ($\mu A\ mM^{-1}\ cm^{-2}$) | LOD (μM) | Ref. |
|---|---|---|---|---|
| $Cu_2O$ NCs/GCE/Nafion | 0.00–0.50 | 121.7[a] | 38.00 | 13 |
| $Cu_2O$ nanospheres/RGOs/GCE | 0.01–6.00 | 185[a] | 0.05 | 14 |
| $Cu_2O$ NCs/GN/GCE | 0.30–3.30 | 28.5 | 3.30 | 55 |
| $Cu_2O$ NCs/Ti | 0.017–11.65 | 28.4 | 15.60 | 15 |
| $Cu_2O$ NCs/$Co_3O_4$ NHs/GCE | 0.001–5.33 | 0.28 | 0.63 | 56 |
| $Cu_2O$-NCs-0/CPE | 0.10–0.70 | 85.6 | 18.0 | This work |
| $Cu_2O$-NCs-0.2/CPE | 0.10–0.70 | 155.2 | 12.0 | This work |
| $Cu_2O$-NCs-1/CPE | 0.10–0.70 | 238.8 | 70.0 | This work |
| $Cu_2O$-NCs-5/CPE | 0.10–0.70 | 135.2 | 38.0 | This work |

[a] Reported as $\mu A\ mM^{-1}$.

$R^2 = 0.9766$ with a sensitivity of 59.7 μA mM$^{-1}$ (238.8 μA mM$^{-1}$ cm$^{-2}$, considering the electrode geometrical area) and a limit of detection (LOD) of 70.0 μM. These experimental parameters are relevant for the application of the method for detecting glucose in biological samples, *e.g.*, human salivary glucose (68 ± 29 μM and 234 ± 200 μM for healthy individuals and patients diagnosed with type 2 diabetes mellitus, respectively).[53] This electrochemical performance is similar, or even higher in comparison to different reported $Cu_2O$-based nanomaterials for non-enzymatic glucose sensing (Table 3).

The remaining $Cu_2O$ NCs samples in non-enzymatic glucose sensing were also tested, obtaining the calibration curves

depicted in Fig. 10, from which the sensitivity was calculated considering the geometrical areas of the electrodes (Table 3). The $Cu_2O$ NCs/CPE based on $Cu_2O$ NCs without starch ($Cu_2O$-NCs-0) had a sensitivity of 85.6 $\mu A\ mM^{-1}\ cm^{-2}$ with LOD = 18.0 $\mu M$ (Fig. 10a). Meanwhile, the modified CPE with $Cu_2O$ NCs synthesized with starch presented higher sensitivities as 155.2 and 135.2 $\mu A\ mM^{-1}\ cm^{-2}$ with a LOD of 12.0 and 38.0 $\mu M$ for $Cu_2O$-NCs-0.2 and $Cu_2O$-NCs-5, respectively (Fig. 10b and d, and Table 3). In all cases, the experimental data were also adjusted using a non-linear fit related to a Langmuir expression (see Fig. S12 and Table S2 in ESI†).

It is important to notice that the sensitivity of the electrocatalysts based on relatively smaller starch-capped $Cu_2O$ NCs was 1.5 to 2.9 times higher than the starch free $Cu_2O$-based working electrode. In general, these results are consistent with the enhanced electrocatalytic activity expected for relatively smaller $Cu_2O$ nanostructures.[54] However, in particular, the starch–$Cu_2O$ nanocomposites did not follow the expected monotonic behavior in terms of their relative particle sizes. A lack of any specific trend was also reported in the degradation of methyl orange (MO) in the presence of starch-stabilized $Cu_2O$ microcrystal-based photocatalysts of different particle sizes.[32]

# 4 Conclusions

In this work, $Cu_2O$ nanocubes ($Cu_2O$ NCs) were successfully synthesized by a green method that includes Benedict's reagent as the copper precursor, D-(+)-galactose as the reducing agent and starch as the capping agent. The synthesized $Cu_2O$ NCs showed a cubic crystalline structure and a high crystallographic purity. The mean particle size values were starch concentration dependent, i.e., the values ranged from 227 to 123 nm in the absence of starch and at the highest amount of starch solution in the synthesis, respectively. In consequence, the electrochemical responses of the $Cu_2O$ NCs-modified carbon paste electrodes were starch concentration dependent too, i.e., an increment of the current for the electrochemical glucose oxidation process was observed when smaller $Cu_2O$ NCs were used. In addition, glucose was quantified by a potentiodynamic method in the range 100–700 $\mu M$ with a sensitivity from 85.6 to 238.8 $\mu A\ mM^{-1}\ cm^{-2}$. Further experimentation to incorporate the presented electrochemical system in a point of care glucose device is taking place in our research group that may enable us to develop a direct non-enzymatic method suitable for glucose detection in real biological specimens.

## Author contributions

Antonio Jiménez-Rodríguez: investigation, validation, visualization, writing – original draft. Eduardo Sotelo: investigation. Lidia Martínez: investigation, visualization, writing – review and editing. Yves Huttel: investigation, writing – review and editing. Maria Ujué González: investigation, visualization, writing – review and editing. Alvaro Mayoral: investigation, visualization, writing – review and editing. Jose Miguel García-Martín: supervision, writing – review and editing, funding acquisition. Marcelo Videa: conceptualization, methodology, writing – review and editing. Jorge L. Cholula-Díaz: supervision, conceptualization, methodology, writing – review and editing, funding acquisition.

## Conflicts of interest

There are no conflicts to declare.

## Acknowledgements

## Notes and references

1 L. A. Terry, S. F. White and L. J. Tigwell, *J. Agric. Food Chem.*, 2005, **53**, 1309–1316.

2 W. Lu, Y. Sun, H. Dai, P. Ni, S. Jiang, Y. Wang, Z. Li and Z. Li, *Sens. Actuators, B*, 2016, **231**, 860–866.

3 K. Ghanbari and Z. Babaei, *Anal. Biochem.*, 2016, **498**, 37–46.

4 R.-m. Yuan, H.-j. Li, X.-m. Yin, J.-h. Lu and L.-l. Zhang, *Talanta*, 2017, **174**, 514–520.

5 W. Villena Gonzales, A. Toaha Mobashsher and A. Abbosh, *Sensors*, 2019, **19**, 800.

6 Y. Su, H. Guo, Z. Wang, Y. Long, W. Li and Y. Tu, *Sens. Actuators, B*, 2018, **255**, 2510–2519.

7 Y. Zhang, Y. Liu, L. Su, Z. Zhang and D. Huo, *Sens. Actuators, B*, 2014, **191**, 86–93.

8 P. Gao and D. Liu, *Sens. Actuators, B*, 2015, **208**, 346–354.

9 L. F. de Castro, S. V. de Freitas, L. C. Duarte, J. A. C. de Souza, T. R. L. C. Paixão and W. K. T. Coltro, *Anal. Bioanal. Chem.*, 2019, **411**, 4919–4928.

10 D. Xu, C. Zhu, X. Meng, Z. Chen, Y. Li, D. Zhang and S. Zhu, *Sens. Actuators, B*, 2018, **265**, 435–442.

11 W. Zhang, Y. Du and M. L. Wang, *Sens. Biosens. Res.*, 2015, **4**, 23–29.

12 J. Yang, W.-D. Zhang and S. Gunasekaran, *Biosens. Bioelectron.*, 2010, **26**, 279–284.

13 S. Felix, P. Kollu and B. P. C. Raghupathy, *J. Chem. Sci.*, 2014, **126**, 25–32.

14 D.-L. Zhou, J.-J. Feng, L.-Y. Cai, Q.-X. Fang, J.-R. Chen and A.-J. Wang, *Electrochim. Acta*, 2014, **115**, 103–108.

15 J. L. K. Jayasingha, M. N. Kaumal, K. M. D. C. Jayathilaka, M. S. Gunewardene, D. P. Dissanayake, J. K. D. S. Jayanetti and I. Cu, *Phys. Status Solidi A*, 2017, **1700135**, 2–8.

16 Q. Li, P. Xu, B. Zhang, H. Tsai, S. Zheng, G. Wu and H.-l. Wang, *J. Phys. Chem. C*, 2013, **117**, 13872–13878.

17 K. Kaviyarasan, S. Anandan and R. Viswanathan, *Ultrason. Sonochem.*, 2016, **29**, 388–393.

18 H. Liu, Z. Hu, R. Hu, B. Liu, H. Ruan, L. Zhang and W. Xiao, *Int. J. Electrochem. Sci.*, 2016, **11**, 2756–2761.

19 Y. Cao, Y. Xu, H. Hao and G. Zhang, *Mater. Lett.*, 2014, **114**, 88–91.

20 P. Raveendran, J. Fu and S. L. Wallen, *J. Am. Chem. Soc.*, 2003, **125**, 13940–13941.

21 V. V. Thekkae Padil and M. Černík, *Int. J. Nanomed.*, 2013, **8**, 889–898.

22 H. Duan, D. Wang and Y. Li, *Chem. Soc. Rev.*, 2015, **44**, 5778–5792.

23 B. Lalithadevi, K. M. Rao and D. Ramananda, *Chem. Phys. Lett.*, 2018, **700**, 74–79.

24 Z. Sabouri, A. Akbari, H. Ali and M. Darroudi, *J. Mol. Struct.*, 2018, **1173**, 931–936.

25 O. S. Oluwafemi, N. Vuyelwa, M. Scriba and S. P. Songca, *Mater. Lett.*, 2013, **106**, 332–336.

26 R. Zamiri, A. Zakaria, H. Abbastabar, M. Darroudi, A. Khorsand and G. P. C. Drummen, *J. Alloys Compd.*, 2012, **516**, 41–48.

27 A. Hebeish, T. I. Shaheen and M. E. El-Naggar, *Int. J. Biol. Macromol.*, 2016, **87**, 70–76.

28 D. Lomelí-Marroquín, D. Medina Cruz, A. Nieto-Argüello, A. Vernet Crua, J. Chen, A. Torres-Castro, T. J. Webster and J. L. Cholula-Díaz, *Int. J. Nanomed.*, 2019, **14**, 2171–2190.

29 A. Vernet Crua, D. Medina, B. Zhang, M. Ujué González, Y. Huttel, J. M. García-Martín, J. L. Cholula-Díaz and T. J. Webster, *Int. J. Nanomed.*, 2019, **14**, 3155–3176.

30 K. Chen and D. Xue, *CrystEngComm*, 2012, **14**, 8068–8075.

31 D. Sun, Y. Du, X. Tian, Z. Li, Z. Chen and C. Zhu, *Mater. Res. Bull.*, 2014, **60**, 704–708.

32 D. Sun, Y. Du, Z. Li, Z. Chen and C. Zhu, *J. Sol-Gel Sci. Technol.*, 2016, 10–12.

33 N. E. Markina, M. V. Pozharov and A. V. Markin, *J. Chem. Educ.*, 2016, **93**, 704–707.

34 W.-c. Huang, L.-m. Lyu, Y.-c. Yang and M. H. Huang, *J. Am. Chem. Soc.*, 2012, **134**, 1261–1267.

35 J. Graves, E. Latvytė, A. Greenwood and N. Emekwuru, *Ultrason. Sonochem.*, 2019, **55**, 25–31.

36 L. O. Cinteza, C. Scomoroscenco, S. N. Voicu, C. L. Nistor, S. G. Nitu, B. Trica, M. L. Jecu and C. Petcu, *Nanomaterials*, 2018, **8**, 1–16.

37 C. F. MacRae, I. Sovago, S. J. Cottrell, P. T. Galek, P. McCabe, E. Pidcock, M. Platings, G. P. Shields, J. S. Stevens, M. Towler and P. A. Wood, *J. Appl. Crystallogr.*, 2020, **53**, 226–235.

38 A. Kirfel and K. Eichhorn, *Acta Crystallogr., Sect. A: Found. Crystallogr.*, 1990, **46**, 271–284.

39 S. Singh, N. Kumar, M. Kumar, A. Agarwal and B. Mizaikoff, *Chem. Eng. J.*, 2017, **313**, 283–292.

40 M. I. Nabila and K. Kannabiran, *Biocatal. Agric. Biotechnol.*, 2018, **15**, 56–62.

41 L. Tang, J. Lv, C. Kong, Z. Yang and J. Li, *New J. Chem.*, 2016, **40**, 6573–6576.

42 F. J. Warren, M. J. Gidley and B. M. Flanagan, *Carbohydr. Polym.*, 2016, **139**, 35–42.

43 J. M. Fang, P. A. Fowler, J. Tomkinson and C. A. S. Hill, *Carbohydr. Polym.*, 2002, **47**, 245–252.

44 R. Kizil, J. Irudayaraj and K. Seetharaman, *J. Agric. Food Chem.*, 2002, **50**, 3912–3918.

45 I. Dankar, A. Haddarah, F. E. L. Omar and F. Sepulcre, *Food Chem.*, 2018, **260**, 7–12.

46 S. Kumar, A. K. Ojha, D. Bhorolua, J. Das and A. Kumar, *Phys. B*, 2019, **558**, 74–81.

47 P. N. Sibiya, T. Xaba and M. J. Moloto, *Pure Appl. Chem.*, 2016, **88**, 61–69.

48 S. Kumar, C. M. Parlett, M. A. Isaacs, D. V. Jowett, R. E. Douthwaite, M. C. Cockett and A. F. Lee, *Appl. Catal., B*, 2016, **189**, 226–232.

49 J. Ghijsen, L. H. Tjeng, J. van Elp, H. Eskes, J. Westerink, G. A. Sawatzky and M. T. Czyzyk, *Phys. Rev. B: Condens. Matter Mater. Phys.*, 1988, **38**, 11322–11330.

50 S. Poulston, P. M. Parlett, P. Stone and M. Bowker, *Surf. Interface Anal.*, 1996, **24**, 811–820.

51 G. Beamson and D. Briggs, *High Resolution XPS of Organic Polymers: The Scienta ESCA300 Database*, Wiley, 1992.

52 K. Sharma, K. Maiti, N. Hoon, D. Hui and J. Hee, *Composites, Part B*, 2018, **138**, 35–44.

53 P. Abikshyeet, V. Ramesh and N. Oza, *Diabetes, Metab. Syndr. Obes.: Targets Ther.*, 2012, **5**, 149–154.

54 X. Yan, J. Yang, L. Ma, X. Tong, Y. Wang and G. Jin, *J. Solid State Electrochem.*, 2015, **19**, 3195–3199.

55 M. Liu, R. Liu and W. Chen, *Biosens. Bioelectron.*, 2013, **45**, 206–212.

56 S. Velmurgan, R. Devasenathipathy, S. M. Chen and S. F. Wang, *Electroanalysis*, 2016, **28**, 1547–1552.